Rheol Acta (2004) 43: 350–363
DOI 10.1007/s00397-003-0350-7

ORIGINAL CONTRIBUTION

Simon J. Haward
Jeffrey A. Odell

Molecular orientation in non-Newtonian flow of dilute polymer solutions around spheres

Received: 16 April 2003
Accepted: 17 November 2003
Published online: 4 February 2004

S. J. Haward · J. A. Odell (✉)
H.H. Wills Physics Dept.,
University of Bristol,
Tyndall Avenue,
Bristol, BS8 1TL, UK
E-mail: jeff.odell@bristol.ac.uk

Abstract A novel approach is presented to study the benchmark problem of flow around spheres in model dilute solutions of monodisperse samples of atactic polystyrene in di-octyl phthalate. Spheres are held ''stationary'' on flexible cantilevers of known spring-constant, k, while the polymer solutions are pumped past at controlled flow rates, allowing access to a wide range of Deborah number. In this way the non-Newtonian forces experienced by the spheres can be measured as a function of Deborah number, while detailed observations and measurements of birefringence are made, enabling assessment of macromolecular strain and orientation. In addition the flow field around a sphere has been measured in an a-PS solution. Experiments have been performed on a single sphere and on two spheres axially aligned in the direction of flow. The extensional flow around the downstream stagnation point of the single sphere is found to play a pivotal role in the development of molecular strain and stress, resulting in flow modification and subsequent non-Newtonian behaviour. The flow birefringence in the wake is found to modify severely the flow around a second, downstream, sphere, affecting the non-Newtonian forces encountered by the second sphere. This provides an explanation for the time interval dependent terminal velocity often observed when two spheres follow the same path through viscoelastic liquids.

Keywords Birefringence · Polymer solution · Extensional flow · Sphere · Stagnation point

Introduction

The motion of spheres in non-Newtonian liquids is of widespread and fundamental importance to many complex industrial processes. In the oil, paint, detergent and cosmetic industries, for example, there is the problem of controlling the settling and suspension of particles in non-Newtonian media. Study of the flow around a sphere can also benefit the understanding of complex cyclic flows such as flow through porous media, which are usually modelled experimentally by packed beds of spheres. This aspect of flow around spheres has relevance to gel permeation chromatography (GPC), filtration of polymer solutions, and enhanced oil recovery (EOR).

The specific case of a sphere settling under gravity along the axis of a cylindrical tube of twice the radius of the sphere has been chosen as a benchmark problem in viscoelastic flow (Leal et al. 1988). However, the transience of this experiment (including a slow approach to steady state), difficulties with experimental reproducibility and a severely limited range of possible flow regimes (due to the reliance on gravity to generate the flow field) are some of the main reasons why

understanding of the physics of the problem has remained limited.

In this paper a new experimental approach is described, in which the flow of polymer solutions around spheres can be studied in steady state, allowing more detailed observations to be made of non-Newtonian flow effects. Flow cells have been constructed in which spheres are held on fine flexible cantilevers of measured spring constant. This allows the forces experienced by the spheres to be measured as a function of the flow rate of the polymer solution, while simultaneous measurements of birefringence and/or the flow field can also be made.

Dilute solutions of monodisperse atactic polystyrene (a-PS) in di-octyl phthalate (DOP) have been studied in the flow cells. Use of such model solutions allows accurate determination of molecular parameters such as contour length and relaxation time, which in turn enables accurate definition of the Deborah number, *De*, of the flow regime. Use of a viscous solvent (DOP) means that shear thinning of the solutions should be negligible and also that inertial effects should be minimal due to the resulting low Reynolds number. Also, since the a-PS molecule has a high intrinsic birefringence, estimates of the molecular strain can be made even at high dilutions.

Background

The falling ball has been found to provide a reliable technique for measuring the shear viscosity of non-Newtonian liquids in the low shear rate limit, with a calculation based on the assumption of Stokes' law (Gottlieb 1979; Chhabra and Uhlherr 1979). However, as detailed below, experiments at higher shear rates have revealed a host of largely unexplained non-Newtonian phenomena that, in many cases, make the acquisition of reproducible experimental results a virtual impossibility.

Bisgaard (1983) used laser-Doppler velocimetry to measure the fluid velocity along the axes of spheres falling through a 1% solution of polyacrylamide in glycerol. Spheres of various sizes and materials were used to provide a variety of sphere terminal velocities. It was found that to get reproducible results in the experiments a long time interval was required between dropping spheres through the solution. More specifically, releasing balls every 10 min resulted in a gradual increase in the terminal velocity of each successive ball until subsequent spheres fell up to 30% faster than the first. Releasing one ball every hour resulted in a velocity increase of up to 9% and an interval of 2.5 h was required before the velocity increase reached less than 2%. Bisgaard noted that viscous heating of the test fluid by the spheres is unlikely to explain a 30% increase in velocity.

Cho et al. (1984) assessed the use of the falling ball as a viscometer for non-Newtonian liquids in the intermediate shear rate range. In aqueous polyacrylamide solutions at concentrations 0.2%, 0.35%, 0.5% and 1% it was found that the terminal velocity was sensitive to the time interval between the dropping of successive balls. When balls were dropped at 30-s intervals in a 1% solution the terminal velocity increased by $\sim$50%. An interval of over 30 min was required to eliminate the effect. Cho et al. pointed out that 30 min was far longer than any usual measure of the relaxation time of the solution.

Jones et al. (1994) found a terminal velocity increase of $>30\%$ for spheres dropped at 15-min intervals in a 0.19% solution of polyisobutylene (PIB) in polybutene (PB), a non-shear thinning Boger fluid. A period of 24 h was required before the solution recovered its original behaviour. The authors did not discover the reason for the velocity increase but stated that it obviously involves some changes in the polymer configuration and that such a possibility could involve the production of extended chain configurations by the passage of the balls. The extended configurations then return to their equilibrium state over a long time period.

Using the same Boger fluids as Jones et al. (1994), Degand and Walters (1995) studied flow around a sphere using a novel approach. A single sphere was held stationary inside a tube as the fluid was driven past using either a pump or a pressure drive or gravity to generate the flow. With this method the authors could access a far greater range of Deborah numbers than with falling balls as the flow velocity could be easily increased and decreased as required. Measurements of the pressure difference across the sphere as a function of flow rate allowed the authors to calculate the drag coefficient. The observation of a sudden increase in the drag coefficient at an onset Deborah number was considered to be certainly due to extensional viscosity effects. It should be noted that this experiment was performed for the special case of the sphere fitting very tightly inside the tube (the ratio of sphere radius to tube radius was 0.88). In this situation there will have been a large component of simple shear in the flow around the sides of the sphere; however the use of Boger fluids should have obviated any effects of this, and the authors observed little shear thinning in their experiments.

Arigo et al. (1995) used laser-Doppler velocimetry to measure the axial velocity along the axis of spheres falling in PIB/PB-based Boger fluid for a range of *De*. They found that the axial velocity profiles remained symmetric in front of and behind the sphere at low *De*. As *De* was increased the upstream velocity profile remained independent of *De*; however downstream of the sphere a wake developed that increased in spatial extent with increasing *De*. At $De\sim7.5$ the wake extended nearly 30 sphere radii behind the sphere, measured to the point where the velocity reached zero; however off axis measurements indicated that, radially, the wake only extended to $\sim$1.1 sphere radii away from the centreline.

The work of Solomon and Muller (1996) involved the settling of spheres in monodisperse polystyrene based Boger fluids. A polystyrene sample of $M_w = 20\times10^6$ was prepared in 0.16% solutions in mixtures of DOP/oligomeric polystyrene and tricresyl phosphate/oligomeric polystyrene to produce solutions of "poor" and "good" extensibility, respectively. The Deborah number of the experiment was varied by using spheres of various densities and sizes. The two fluids showed drag increases of $>300\%$ for $De>1$, an effect considered by the authors to be purely elastic since the Reynolds number was <0.01.

Fabris et al. (1999) used digital particle image velocimetry to perform measurements of the flow field around falling spheres in the solution of "good" extensibility studied by Solomon and Muller (1996). Fabris et al. found that the radial part of the flow field remained symmetric as *De* increased and was very similar to the flow field observed in glycerol. The axial component, however, remained constant in front of the ball but developed an increasingly long trailing wake with increasing *De*. A large increase in the drag coefficient was observed with increasing *De*, and both this and the observed flow field modification were attributed to an increase in extensional viscosity along the centreline of the trailing wake.

The computational work of Chilcott and Rallison (1988) concerning the flow of a suspension of FENE-CR dumbbells past a rigid sphere showed that, for high *De*, the polymer became highly stretched in thin regions of fluid close to and downstream of the rear stagnation point.

Harlen (1990) modelled the steady flow of a polymer solution past a sphere falling at high *De* but low *Re* using the birefringent strand technique developed by Harlen et al. (1990). The presence of a thin strand of highly extended polymer downstream of the sphere caused the velocity in the wake to decay much more slowly than for a Newtonian fluid and produced an increase in the drag coefficient. The form of the downstream wake was comparable to that measured by Bisgaard (1983).

In the present paper we report flow effects and their interaction with molecular orientation around a single sphere. We also report how the wake of a single sphere can affect a second sphere, downstream of the first, and axially aligned in the direction of flow. Such a study should shed light on the still largely unexplained time-dependent "velocity effect", which has been observed when two or more spheres follow the same path through a polymer solution (Bisgaard 1983; Cho et al. 1984; Jones et al. 1994), reviewed above. These previous studies have been performed with a wide range of concentrations (generally semi-dilute or concentrated) in highly viscous solvents of variable quality. All of these factors can cause the effective orientational relaxation time to vary by orders of magnitude. In this paper we shall concentrate upon the well-defined problem of dilute theta solutions of well-defined monodisperse polymers in a relatively inviscous solvent.

The understanding of how two aligned particles may interact in polymeric liquids has clear relevance to understanding porous media flows, since porous media are usually modelled in the laboratory by beds packed with spheres. The relevance to particle settling and suspensions is also clear.

Experimental

Apparatus The "single sphere" and "double sphere" flow cells used in the experiments are shown schematically in Fig. 1. The walls of the cells were cut from a 4 mm thick sheet of soda glass, which had been annealed to improve its optical isotropy, and were bonded together into square tubes of 100mm^2 cross-section (inside) using an inert silicon based adhesive. One of the walls of each cell had a 10 mm diameter hole cut through it to allow the insertion of the sphere/cantilever assembly.

The glass spheres were of diameter 2 ± 0.02 mm and were supplied by Sigmund-Lindner of Germany. The spheres were each glued to one end of a cantilever cut from a length of flexible optic fibre of diameter 125 ± 2 μm. The opposite end of the cantilever was fixed rigidly into one end of a 10 mm diameter glass cylinder. The lengths of the cantilever and the cylinder were such that, when the spheres were inserted into the cell and the cylinder was secured to the cell wall, the rest position of the spheres was on the central axis of the flow cell. In the double sphere flow cell the spheres were separated by a centre-centre distance of ~5 mm.

The cantilevers were cut to a length of ~19 mm, to provide a spring constant, *k*, of ~0.4 Nm^{-1} to provide a measurable displacement of the spheres in the flowing solvent. The spring constant of the cantilever was measured approximately, before the sphere was attached, by holding the cantilever in a horizontal position and measuring the vertical displacement of the free end of the cantilever as increasing weights were added to it. By ensuring the range of cantilever deflection was greater than would occur under experimental conditions, this measurement of *k* also ensured that *k* would be constant over the experimental range of movement. A more accurate value for the spring constant was determined with the sphere and cantilever "in situ" by attaching the flow cell rigidly to a

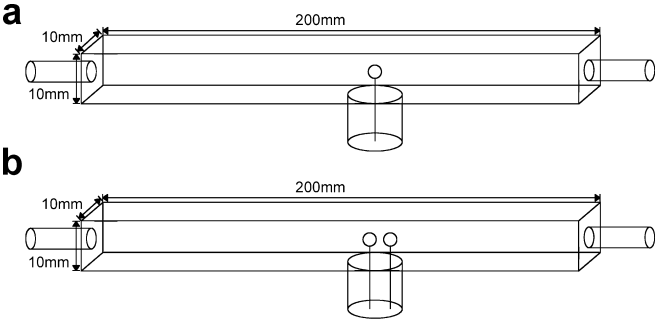

Fig. 1 **a** Schematic diagram of the single sphere flow cell. **b** Schematic diagram of the double sphere flow cell (the centre-centre spacing between spheres was ~5 mm)

magnetic coil driven by a signal generator and exciting the first natural resonant frequency, ω, of the cantilever. The corresponding spring constant was calculated using $\omega = \sqrt{k/m}$, where m is the mass of the sphere.

All of the dimensions of the flow cell were carefully calculated to provide a good range of strain rate and an easily measurable cantilever deflection in the given solvents and at the available flow rates while, at the same time, minimising the volume of solution required per experiment and also minimising wall effects.

The flow cells were incorporated into the apparatus shown schematically in Fig. 2. The polymer solution (or solvent) was drawn through the test cell from reservoir 1 to reservoir 2 by the vacuum pump. The volume flow rate was controlled by adjusting valves 1 and 2 to control the vacuum pressure inside reservoir 2 and was calculated from a measurement of the pressure drop, ΔP, across a calibrated capillary connected to reservoir 1. When an experiment had been completed valve 3 was closed to stop the flow and the vacuum was switched off. The liquid in reservoir 2 could then be either returned to reservoir 1 by opening valve 4, or could be discarded to waste.

The spheres inside the flow cells were viewed using a cooled C.C.D. camera interfaced to a PC, allowing the displacement of the spheres to be measured directly, and allowing individual photo frames and sequences to be captured. The test cells were mounted on a translation stage to allow adjustments to be made for the displacement of the spheres when the cantilevers bent in the flowing liquid. The cantilever bend inevitably introduced a small degree of error into the experiment because the spheres were pulled slightly away from the flow axis causing asymmetry in the flow field. The maximum deviation of the sphere from the flow axis occurred at the highest flow rates in viscous solutions and was ~0.5 sphere radii. In the double sphere flow-cell the different displacement of each sphere caused them to become slightly non-colinear. The typical difference in axial position corresponded to 1/60 of a radius, reaching a maximum of 1/10 radius for high flow-rates of viscous solutions.

Force measurement and estimation of specific viscosity The force, F, upon each sphere was measured for polymer solutions, $F_{solution}$, and for the pure solvent, $F_{solvent}$ as a function of the superficial flow velocity. Since Stokes' law relates the force felt by a sphere to the viscosity of the fluid in which the sphere is moving an estimate of the specific viscosity, η_{sp}, of the polymer solutions was made at a given flow rate simply by

$$\eta_{sp} = \frac{F_{solution} - F_{solvent}}{F_{solvent}} \tag{1}$$

This method has some important advantages over other approaches. Since the flow is unlikely to be strictly creeping flow, i.e. since the Reynolds' number will be greater than zero, corrections ought to be made to both $F_{solution}$ and $F_{solvent}$ due to inertial forces. However, since the inertial force contributions to $F_{solution}$ and $F_{solvent}$ should be essentially equal, the process of subtraction in Eq. (1) should largely obviate errors due to these effects. Also, since the solvent specific viscosity is identically equal to zero, polymer effects (i.e. shear thinning or the increase in extensional viscosity) should be clear when η_{sp} is plotted as a function of strain rate or Deborah number. In the double sphere flow cell, the application of Eq. (1) to each sphere separately should also obviate the effects of slipstreaming.

The superficial flow velocity, v, was calculated from the measurement of volume flow rate divided by the cross-sectional area of the flow cell. This value of v was used in the calculation of Reynolds number, Re, according to

$$Re = \frac{\rho v r}{\eta} \tag{2}$$

where r is the radius of the sphere and ρ and η are the density and viscosity of the solvent, respectively. For polymer solutions the strain rate was determined by

$$\dot{\varepsilon} \approx \frac{v}{r} \tag{3}$$

The Deborah number was determined using

$$De \approx \frac{\tau v}{r} = \tau \dot{\varepsilon} \tag{4}$$

where τ is taken as the longest molecular, Zimm, relaxation time. The relaxation times of the polymer samples used in the experiments are discussed below.

Observation and estimation of birefringence Birefringence in the flow cells was detected using the optical system illustrated schematically in Fig. 3. A 4-mW helium-neon laser was positioned such that the beam passed orthogonally through the walls of the flow cell and the observation area (the trailing stagnation point of a sphere). The laser beam was detected by the cooled C.C.D. camera,

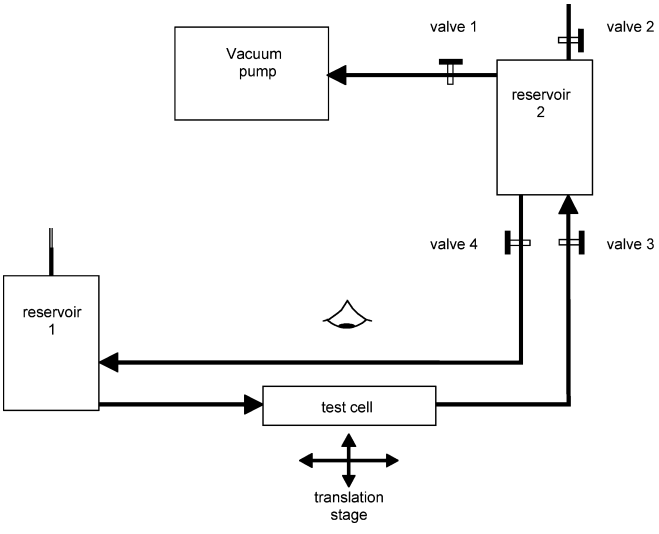

Fig. 2 Vacuum driven flow system

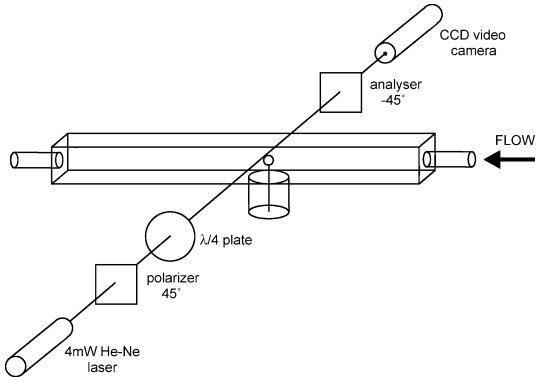

Fig. 3 Optical system used to measure birefringence in the single sphere flow cell

which was focussed on the stagnation point area. The polarizer and analyser were placed on either side of the flow cell with their axes at 45° to the flow axis and at 90° to each other to minimize the signal received by the C.C.D. camera. A $\lambda/4$ plate was inserted between the polarizer and analyser to compensate for residual birefringence in the glass walls of the cell. The $\lambda/4$ plate was rotated to achieve the minimum signal and the polarizer and analyser were readjusted iteratively to achieve extinction of the beam.

During experiments with polymer solutions, 25-ms images were captured for a range of flow rates. When the flow was stopped a 25-ms background image was captured. The background image was subtracted from the images captured under flow to reveal the birefringent signal. This was done within 1 s to provide the best possible background image for subtraction.

The intensity of the detected signal was calibrated by placing a $\lambda/30$ compensator in the optical line shown in Fig. 3. The change in the signal intensity was measured as the compensator was rotated to produce a range of retardation values.

The retardation, R, is related to the birefringence, Δn, by

$$R = \Delta n l \tag{5}$$

where l is the path-length through the birefringent material. Note that some previous authors have used an algorithm to de-convolve the cylindrical symmetry of birefringent lines observed in opposed jet flow (Cathey and Fuller 1990; Carrington et al. 1997a, 1997b). This was inappropriate for the present study, since the birefringence observed here was not necessarily symmetric about the flow axis and frequently became unstable (i.e. fluctuated with time) at high flow rates.

Flow visualization Flow visualization experiments were performed in the single sphere flow cell using a modification to the optical system illustrated in Fig. 3. Two orthogonal cylindrical lenses were positioned so as to focus the laser beam into a very narrow plane ($\sim$100 μm) that passed through the observation area, bisecting the sphere. The C.C.D. camera was positioned at 90° to the plane of the light and was focussed on the observation area to receive light scattered from latex tracer particles suspended in the fluid.

Images were captured and the local fluid velocity around the sphere was resolved in the direction of the flow axis using the known exposure time of the image and the lengths of the streaks created by the tracer particles.

Polymer solutions Dilute solutions of mono-disperse atactic poly(styrene) in di-octyl phthalate (a-PS in DOP) were employed in the experiments. DOP is a viscous, low molecular weight, solvent of viscosity $\eta_{DOP} = 0.04$ Pa s (Durrans 1971). The θ-temperature for the a-PS/DOP system is 22 °C (Berry 1967).

Three a-PS samples of molecular weights $M_w = 6.9\times10^6$, $M_w = 8.5\times10^6$ and $M_w = 10.2\times10^6$ were used. The samples, all supplied by Polymer Laboratories, were closely monodisperse, having polydispersity indices, M_w/M_n, of 1.15, 1.2 and 1.17, respectively. Solutions were prepared in concentrations between 0.005 wt% and 0.03 wt%. The solution temperatures were measured prior to experiment to be 22 ± 1 °C.

An estimate of τ for the polymer solutions was determined from experiments on 0.01% solutions of a-PS in DOP using a new technique called "oscillatory extensional rheometry", in which a small volume of fluid is repeatedly oscillated through the stagnation point of a cross-slot device (Carrington et al. 1997a, 1997b; Carrington and Odell 2003). The molecular weights tested were $M_w = 6.9\times10^6$ and $M_w = 10.2\times10^6$ and the solutions were, in fact, identical to those studied here. The intensity of birefringence was measured as a function of strain rate in the oscillatory cross-slots and the critical strain rate, $\dot{\varepsilon}_c = 1/\tau$, of each solution was determined from the points of inflection on the birefringence vs strain rate curves. Such experiments are thought to give reliable estimates of the Zimm relaxation time τ, including hydrodynamic interactions. The estimates of τ for the a-PS solutions, including a linear extrapolation for the $M_w = 8.5\times10^6$ sample, are shown in Table 1, together with calculated values for the Zimm relaxation time, intrinsic viscosities calculated from the Mark-Houwink equation and values of c*. There is reasonable agreement between the calculated and measured values, the measured values being consistently around twice the calculated value. This probably reflects the uncertainty in solvent quality and viscosity and in the polymer physics of the coil-stretch process intrinsic to the technique.

Our estimate of c* concentration was made on the assumption of each molecule occupying the volume of a cube of dimension $2R_g$, i.e.

$$c* = \frac{M_w}{N_A (2R_g)^3} \tag{6}$$

where R_g represents the equilibrium radius of gyration and N_A is Avogadro's number. This assumption yields a considerably lower estimate of c* than the common assumption of each molecule occupying a sphere of radius R_g (e.g. Graessley 1980).

From our conservative estimates of c* given in Table 1 it can be seen that our experimental concentrations lie in the range $c*/42 < c < c*/7$. For all but our highest experimental concentrations, $c < c*/10$. For this reason we consider our test solutions to be highly dilute.

From the values of $[\eta]$ given in Table 1, calculated from the Mark-Houwink coefficients for a-PS in DOP, it can be shown that the relative viscosities of our test solutions lie in the range $1.01 < \eta_{rel} < 1.08$. This indicates that our solutions should not be greatly affected by shear flow and should be expected to behave as non-shear thinning Boger fluids.

Results

Single sphere flow cell

Force measurements and estimates of specific viscosity

Figure 4a shows how the force on the single sphere increases with the Reynolds number in solutions of various concentration of $M_w = 10.2\times10^6$ a-PS in DOP. The force on the sphere in the pure solvent is represented by the solid line in Fig. 4a and is well fitted by a quadratic in *Re*, indicating the presence of low *Re* inertial effects. Increasing departures from the solvent behaviour are observed with increasing polymer concentration and *Re*.

In Fig. 4b the data from Fig. 4a has been converted into a plot of the specific viscosity, η_{sp}, as a function of the Deborah number, *De*, as described above. In this

Table 1 Estimated Zimm relaxation times, theoretical values for the intrinsic viscosities and c* for a-PS/DOP solutions

a-PS molecular weight	6.9×10^6	8.5×10^6	10.2×10^6
Experimental relaxation time, τ (ms) $\pm 20\%$	2.00	2.75	3.60
Calculated Zimm Relaxation time (ms)	1.08	1.49	1.95
$[\eta]$ (Mark-Houwink), $cm^3\ g^{-1}$	210.1	233.2	255.5
C* (wt%)	0.26	0.23	0.21

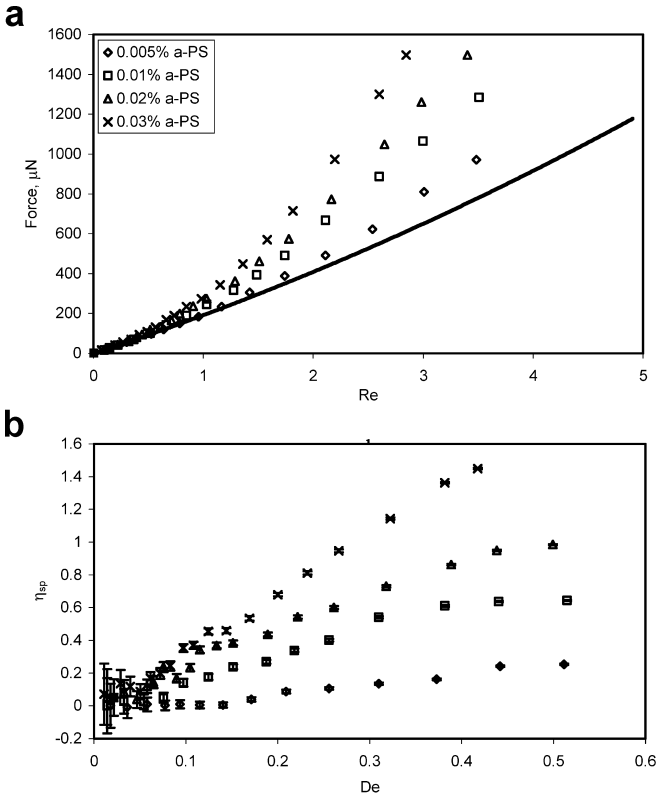

Fig. 4 **a** Force as a function of Reynolds' number in the single sphere cell for solutions of $M_w = 10.2\times10^6$ a-PS in DOP. The *solid line* represents the data obtained from the pure solvent. **b** Specific viscosity as a function of Deborah number in the single sphere cell. Derived from Fig. 4a

plot the solvent curve lies identically along the x-axis, so the departures from Newtonian behaviour due to the polymer additives are much clearer than in Fig. 4a.

The polymer solutions in Fig. 4b display a rapid increase in the specific viscosity above an onset Deborah number, De_o. Below De_o the specific viscosity has an approximately constant value. The increase in specific viscosity tends (except for the highest concentration) towards a plateau value with increasing Deborah number. As expected, the plateau values increase with polymer concentration. It is notable that the value of De_o becomes progressively lower as the polymer concentration is increased. The range of *De* over which the viscosity increase occurs could be considered critical, as even these ''monodisperse'' polymers contain a significant range of molecular weights, corresponding to a range of τ of about 10:1.

Figure 5 shows a comparison between the behaviour of the different molecular weight a-PS samples for a constant concentration of 0.02%. Qualitatively the solutions behave as expected, showing an increase in the maximum specific viscosity with increasing M_w.

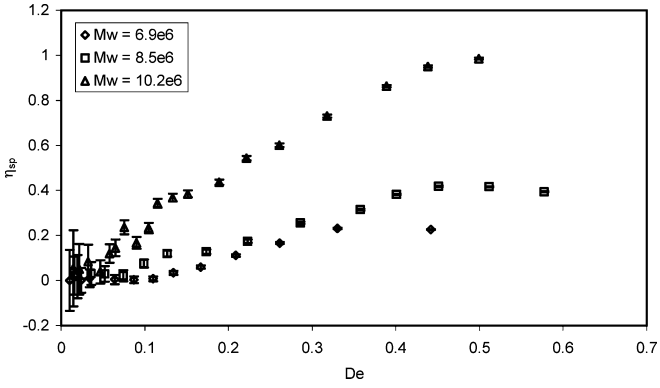

Fig. 5 Specific viscosity as a function of Deborah number in the single sphere cell for 0.02% solutions of a-PS in DOP at the molecular weights indicated

The a-PS solutions display qualitatively similar behaviour at all three molecular weights and concentrations tested. The specific viscosities of the polymer solutions are seen to have an approximately constant, or ''pseudo-Newtonian'', value below an onset Deborah number, De_o. Above the onset Deborah number the specific viscosity rises steadily and tend towards plateau values.

The general behaviour of the a-PS solutions in the single sphere cell is consistent with an increase in the specific viscosity as a result of polymer extension. In fact the curves are comparable in nature to the results of Carrington et al. (1997a, 1997b), who made pressure drop measurements across the opposed jets, which correlated with the increase in molecular strain in a 0.02% solution of $M_w = 8\times10^6$ a-PS in dekalin. These authors suggested that the behaviour was due to the coil↔stretch transition in dilute solutions.

However, the onset Deborah number marking the onset of the viscosity increase in the a-PS/DOP solutions in the single sphere cell is lower than the expected value of $De_o \sim 0.5$–1. Flow field measurements in the single sphere flow cell show that the flow velocity along the symmetry axis may be up to double the superficial flow velocity used to calculate the Deborah number; see below. Also the polydispersity of the a-PS samples, though small, may be significant in showing extension effects at low *De* due to the high molecular weight tail (this may also account for the reduction in De_o with increasing polymer concentration and M_w). Furthermore the flow-field around the sphere is not well enough understood, especially in polymer solutions, to allow an accurate definition of the strain rate and therefore Deborah number. For this reason calculations of strain rate and Deborah number are based purely on the geometry of the flow cell and complications to the flow field are ignored.

Observations and estimates of birefringence

Figure 6 shows the development of birefringence in the trailing wake of the sphere as the Deborah number increases in a 0.02% solution of $M_w = 10.2\times10^6$ a-PS in DOP. At the lowest Deborah numbers ($De = 0.04$, 0.07) no birefringence is visible. At $De = 0.14$ a weak localised birefringent line is visible originating from the stagnation point. The line increases in width and intensity with increasing De until, at $De = 0.29$, two separate lines can clearly be distinguished. With further increases in the Deborah number the structure of the birefringence is seen to become more complicated, consisting of many striations. At high De flow instabilities in the wake became evident as the complex birefringent structure began to fluctuate. The individual strands that form the structure were observed to oscillate in position and intensity as shown in Fig. 7, where successive frames correspond to 200-ms time intervals. The typical timescale for these fluctuations was around 0.25 s, around 200 times the characteristic relaxation time. Such fluctuations were predicted by Harris and Rallison (1994) for moderate De in stagnation point flow of a dilute polymer solution modelled by dumbbells with non-linear hydrodynamic friction. They are thought to arise from a coupling between the stretching of the polymer and consequent modification of the flow-field.

Estimates of the birefringence (Δn) of the strand in the 0.02% solution of $M_w = 10.2\times10^6$ a-PS produced a maximum value at $De = 0.5$ of $\Delta n_{max} \sim 6\times10^{-6}$. This can be compared with a theoretical maximum value of $\Delta n_0 = 1.6\times10^{-5}$, from an expression derived by Peterlin (1961). Using the model of Treloar (1975), based on the segmental isotropy of a strained network, the ratio of Δn_{max} to Δn_0 suggests that the polymer molecules have extended to some 60% of their contour length, i.e. the extension ratio of ~0.6 (see also Carrington et al. 1997a, 1997b). Similar estimates for more dilute solutions ($M_w = 10.2\times10^6$ sample at c = 0.005% and $M_w = 6.9\times10^6$ and $M_w = 8.5\times10^6$ samples at c ≤ 0.01%) yielded maximum extension ratios of ~1 (i.e. full extension) at high De.

Birefringent lines were followed for approximately 5 mm downstream of the trailing stagnation point by slowly moving the flow cell in front of the C.C.D. camera using the translational stage. At the highest experimental flow velocity of ~150 mm s^{-1} this distance represents a time interval of ~0.03 s, almost an order of magnitude longer than the expected relaxation time of the $M_w = 10.2\times10^6$ a-PS sample; see Table 1.

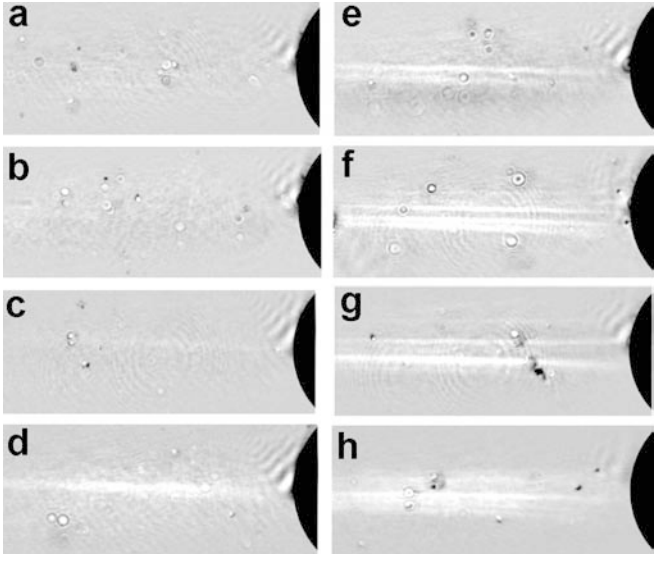

Fig. 6a–h Development of birefringence with strain rate and Deborah number downstream of the stagnation point of the single sphere flow cell. 0.02% $M_w = 10.2\times10^6$ a-PS in DOP: **a** $De = 0.04$; **b** $De = 0.07$; **c** $De = 0.14$; **d** $De = 0.22$; **e** $De = 0.29$; **f** $De = 0.36$; **g** $De = 0.43$; **h** $De = 0.50$. For clarity the position of the sphere is indicated by a *superimposed circular section*. Flow is from right to left

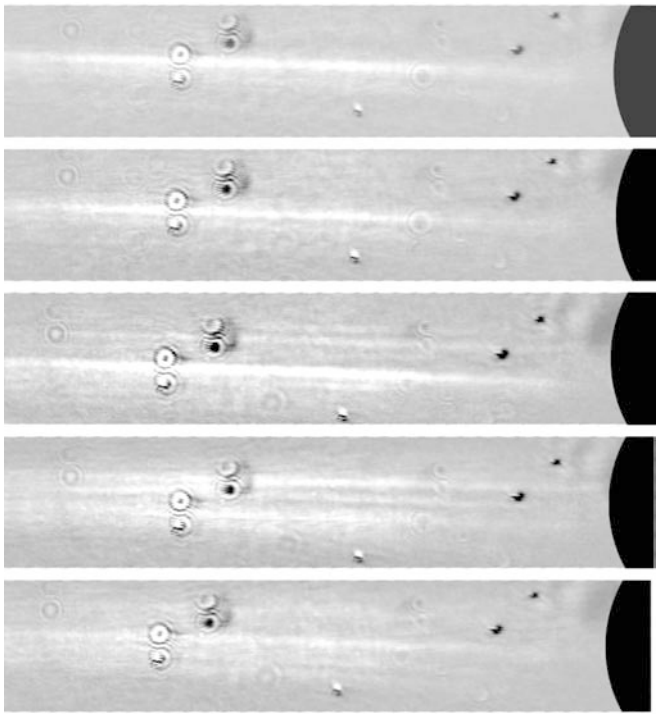

Fig. 7 A selection of images captured within a 1 s time interval that demonstrate the instabilities in the birefringent strands observed in the wake of the sphere. 0.02% solution of $M_w = 10.2\times10^6$ a-PS in DOP at $\dot{\epsilon} = 140\ s^{-1}$ ($De = 0.5$). Flow is from right to left

Flow-field visualisation

Figure 8 shows a sequence of flow field plots for a 0.02% solution of $M_w = 10.2\times10^6$ a-PS in DOP. Vectors are

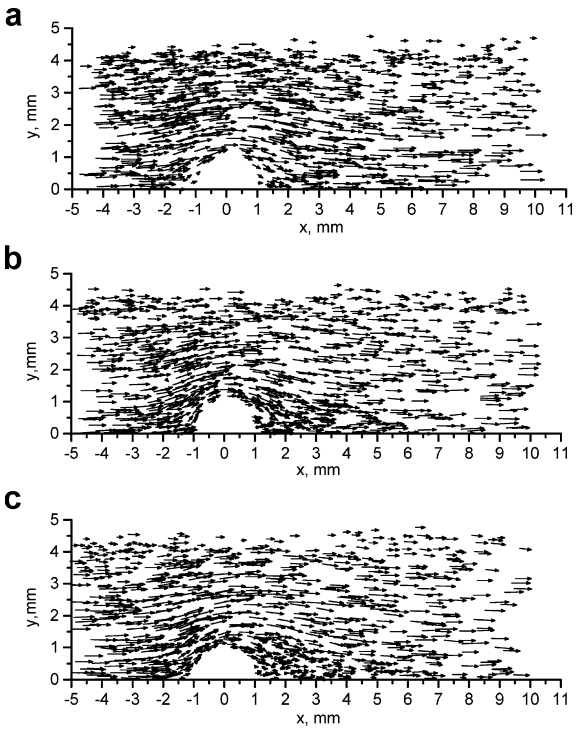

Fig. 8a–c Vector plots of the velocity field around the sphere in the single sphere flow cell for a 0.02% solution of $M_w = 10.2\times10^6$ a-PS in DOP flowing at: **a** $v = 20$ mm s^{-1}; $De = 0.07$; **b** $v = 80$ mm s^{-1}; $De = 0.29$; **c** $v = 160$ mm s^{-1}; $De = 0.58$. Flow is from left to right and the sphere is centred at (0,0). In each case the superficial flow velocity, v, is represented by →

shown corresponding to the flow velocity and direction. At the lowest flow rate of $v = 20$ mm s^{-1} ($De = 0.07$, Fig. 8a) the flow field is seen to be only slightly asymmetric about the x = 0 axis, which is similar to the flow field expected from viscous flow of a Newtonian fluid. As the flow rate is increased to $v = 80$ mm s^{-1} ($De = 0.29$, Fig. 8b); however, a high degree of asymmetry can be observed in front of and behind the sphere. An extended wake has formed downstream of the sphere with very low fluid velocities along the stagnation streamline. At the highest flow rate, $v = 160$ mm s^{-1} ($De = 0.58$, Fig. 8c), the low velocity trailing wake has become very pronounced and extends for nearly eight radii behind the sphere. This is a large perturbation to the flow field observed in Newtonian liquids. In pure DOP, for example, we observed a symmetric flow field around the sphere even at a superficial flow velocity of $v = 200$ mm s^{-1}. Although more qualitative, our results are consistent with those of Fabris et al. (1999).

In the a-PS solutions it is seen that fluid in the trailing wake of the sphere requires a considerable distance, in comparison to the solvent, in which to accelerate away from the stagnation point up to the superficial flow velocity. There are two important consequences of this extended period of fluid acceleration in the wake. The first is a reduction in the value of v/r for the strain rate at the trailing stagnation point. The second is that an extensional component will remain in the flow field on the stagnation point axis for up to several radii downstream of the sphere.

Double sphere flow cell

Force measurements and estimates of specific viscosity

Figure 9a shows the forces measured on each sphere of the double sphere flow cell with a 0.02% solution of $M_w = 10.2\times10^6$ a-PS in DOP, compared to the forces measured in pure DOP. For the solvent the force curve corresponding to the first sphere to encounter the flow, "sphere 1", is well fitted by a quadratic equation in *Re*. The second sphere along the flow axis, "sphere 2", is seen to experience a force that increases linearly with Reynolds' number, indicating an absence of significant fluid inertial contributions to the force. Sphere 2 is seen to experience a reduction in force, compared to sphere 1, for $Re > \sim 0.5$. This is probably due to the onset of inertial effects in the downstream wake of sphere 1 (as

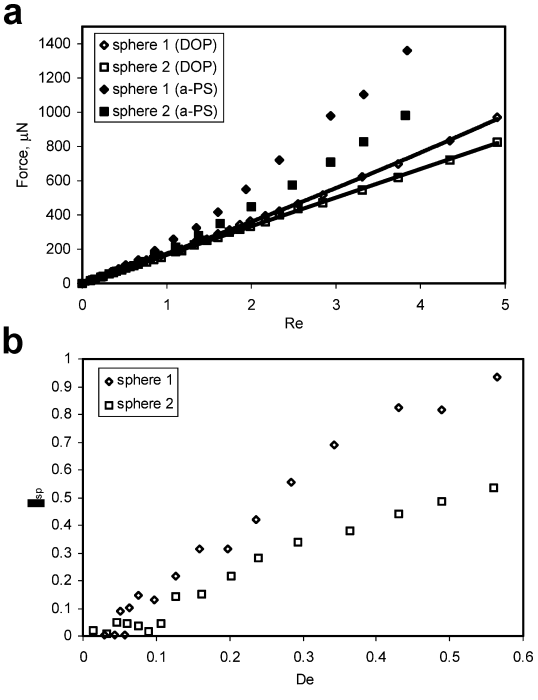

Fig. 9 a Force as a function of Reynolds number, *Re*, for each sphere of the double sphere flow cell in pure DOP and in a 0.02% solution of $M_w = 10.2\times10^6$ a-PS in DOP. The *solid lines* represent a quadratic fit to the data for sphere 1 and a linear fit to the data for sphere 2 in pure DOP. The equations for the lines of best fit are: $F = 5.2Re^2 + 170.4Re$, and $F = 167.4Re$, respectively. **b** Specific viscosity, η_{sp}, as a function of the Deborah number, *De*, derived from Fig. 8a

indicated by the quadratic fit to the force curve) causing a slight reduction in the flow velocity, i.e. a slipstreaming effect.

The polymer solution force curves for each sphere in Fig. 9a appear to follow closely the respective solvent curves until an onset Reynolds' number is reached. Beyond the onset Reynolds' number, which appears to be approximately the same for both spheres, the polymer curves begin to diverge from the solvent curves. The departure from Newtonian behaviour increases with *Re*. Although it is clear that sphere 1 experiences a greater total force than sphere 2 in the polymer solution, it is not entirely clear how much of this extra force arises from the polymer additive to the solvent.

By comparing the polymer curves in Fig. 9a with the solvent curve for the respective sphere, the apparent specific viscosity, $\eta_{sp,}$ has been estimated for each sphere separately using Eq. (1). Thus both solvent curves become identically equal to zero, for all *Re*, removing the slipstreaming effect from the data and making comparisons between the polymer curves much simpler. In Fig. 9b the data from Fig. 9a has been treated in this way and plotted as a function of *De*. The curves for both spheres in Fig. 9b show an increase in the specific viscosity from pseudo-Newtonian behaviour above an onset Deborah number, De_o. The curve obtained from sphere 1 of the double sphere cell is similar to the curve obtained with the same solution in the single sphere flow cell; see above. However it is immediately obvious in Fig. 9b that sphere 2 experiences a significantly lower increase in specific viscosity due to the polymer than sphere 1. Also the apparent onset Deborah number for the viscosity increase is greater for sphere 2 than sphere 1.

With increasing De the curves appear to be tending towards plateau values of $\eta_{sp.}$ The difference in maximum values of η_{sp} in Fig. 9b represents a difference in apparent viscosity of ~40%, i.e. sphere 2 experiences ~40% less force than sphere 1 due to the polymer additive in the solution. This relative reduction in force is entirely analogous to the "velocity effect" observed in falling ball experiments. Since Stokes' law relates the viscous force on a spherical particle to the velocity of the fluid, sphere 2 could be expected to fall ~40% faster than sphere 1, if a falling ball experiment was conducted under identical conditions. In fact the increase in velocity may well be greater than this, since the 40% does not include the Newtonian slipstreaming effect (the total maximum difference in force between the 2 spheres in the 0.02% solution of $M_w = 10.2\times10^6$ a-PS can be estimated from Fig. 9a to be ~55%).

The time for fluid to flow between the spheres is ~0.03 s, which is almost an order of magnitude greater than the longest expected molecular relaxation time of the $M_w = 10.2\times10^6$ a-PS sample ($\tau = 0.0036$ s); Carrington and Odell (2003). However, in relation to falling ball experiments, 0.03 s is an extremely short time interval between spheres, and difficult to achieve experimentally. Though the effect is short-lived in comparison to previous studies (Bisgaard 1983; Cho et al. 1984; Jones et al. 1994), the present system is highly dilute and the solvent relatively inviscous, so that the effect is long-lived in terms of the polymer relaxation time, τ.

Due to the analogy with falling ball experiments the quantity defined by the difference in plateau values of specific viscosity for spheres 1 and 2 will, from now on, be termed the "effective velocity effect" and denoted by Δv_{eff}. Therefore, in Fig. 9b, $\Delta v_{eff} \approx 0.4$, which means that a difference of ~40% was measured in the force exerted by the polymer on each ball.

To show the effect of molecular weight, Fig. 10 shows similar curves to Fig. 9b for a 0.02% solution of $M_w = 6.9\times10^6$ a-PS in DOP. Similar features are observed as for the $M_w = 10.2\times10^6$ solution. There is a small increase in the onset Deborah number between sphere 1 and sphere 2. Both curves rise to plateau values indicating an effective velocity effect of $\Delta v_{eff} \approx 0.15$. It should be noted that the second sphere shows a drop in specific viscosity around a *De* of 0.4. This has been seen a number of times with other solutions. Beyond this value the curves tend towards a plateau value.

Concentration dependence is shown in Fig. 11, which shows the specific viscosity as a function of *De* for a 0.01% solution of $M_w = 10.2\times10^6$ a-PS in DOP. In Fig. 11, Δv_{eff} reaches a maximum value of ~0.25 at $De = 0.5$.

Observations of birefringence

Due to experimental difficulties with calibrating the retardation in the double sphere experiments, quantitative measurements of birefringence were not possible. It was also not possible to obtain background images from positions situated behind sphere 1 of the cell due to the

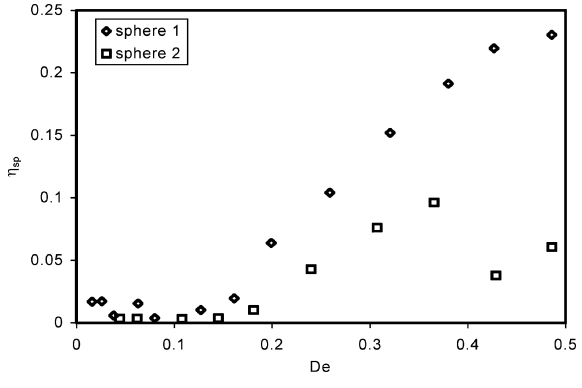

Fig. 10 Specific viscosity, η_{sp}, as a function of the Deborah number, *De*, for the spheres of the double sphere flow cell in a 0.02% solution of $M_w = 6.9\times10^6$ a-PS in DOP

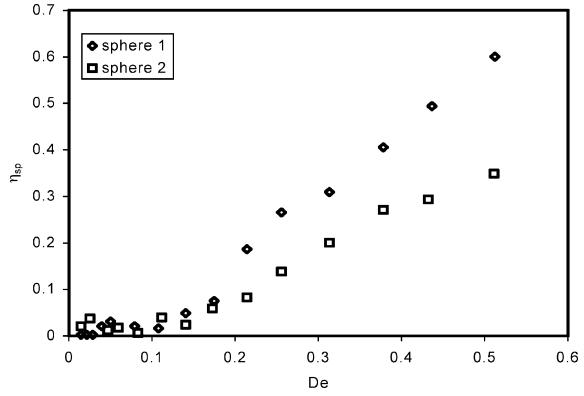

Fig. 11 Specific viscosity, η_{sp}, as a function of the Deborah number, *De*, for the spheres of the double sphere flow cell in a 0.01% solution of $M_w = 10.2\times10^6$ a-PS in DOP

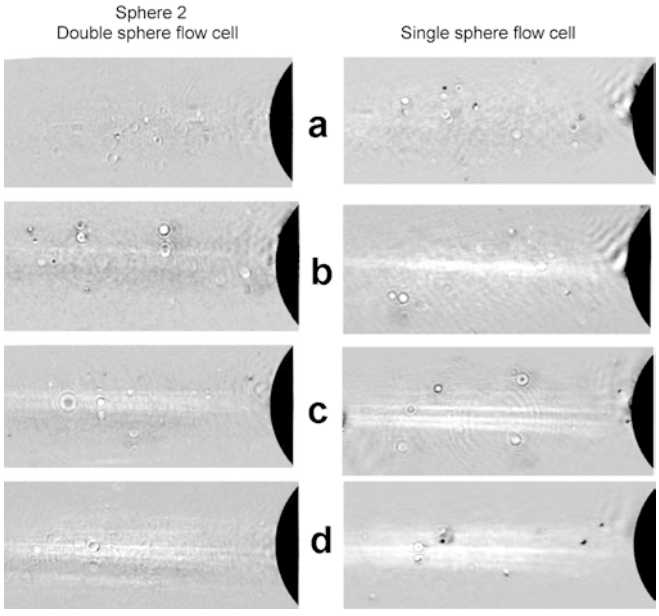

Fig. 12a–d Development of birefringence with *De* in the stagnation point of sphere 2 of the double sphere flow cell in a 0.02% solution of $M_w = 10.2\times10^6$ a-PS in DOP. Shown for comparison is the birefringence observed in the stagnation point of the single sphere in the same solution and for the same values of *De*. *De* =: **a** 0.07; **b** 0.22; **c** 0.36; **d** 0.5. For clarity the position of the sphere is indicated by a *superimposed circular section*. Flow is from right to left

change in position of the spheres with and without flow. Background corrections were possible for images captured from behind sphere 2, however, and comparison of these images with those captured in the single sphere flow cell allow useful insights to be made on the assumption that observations made in the single sphere flow cell would be similar to observations made on sphere 1 of the double sphere flow cell.

Accordingly, Fig. 12 shows a comparison between the birefringence observed at the stagnation point of sphere 2 with that observed at the stagnation point of the single sphere flow cell for a 0.02% solution of $M_w = 10.2\times10^6$ a-PS in DOP. It is apparent that, for a given Deborah number, the birefringent signal detected in the wake of sphere 2 is significantly weaker than the signal observed behind the single sphere. As shown by Fig. 12, the onset Deborah number for the appearance of the birefringent line is greater for sphere 2 than for the single sphere. The onset Deborah number for the observed increase in birefringence broadly corresponds with the Deborah number for the increase in specific viscosity.

The birefringent strands that originated from behind sphere 1 of the double sphere cell were tracked as they flowed into the flow field of sphere 2. Due to the aforementioned difficulties with making background corrections a 0.03% solution of $M_w = 10.2\times10^6$ a-PS in DOP was used and the experiment was conducted at a high strain rate ($\dot{\epsilon} = 250\ s^{-1}$) so that the birefringent signal would be intense and could be seen above the laser background. Even so, individual photo-frames did not show the birefringence clearly; however, when sequences of frames were viewed as videos, the fluctuation of intensity and position of the birefringent lines allowed them to be seen.

Many sequences of frames were captured as the double sphere flow cell was translated past the CCD video camera. Birefringent lines were followed from their origin immediately behind sphere 1, from where they flowed towards sphere 2 in more or less straight lines. Near the leading edge of sphere 2 the lines diverged as if following the streamlines around the surface of the sphere. Approaching sphere 2, the birefringent strands could be seen flowing very closely around the sides of the sphere. Sometimes birefringent lines that had originated from behind sphere 1 could be seen through the glass of sphere 2 as they flowed around the opposite side of the sphere from the CCD camera. The birefringent lines moved erratically around the circumference of sphere 2, probably due to viscoelastic instabilities, see discussion. Immediately behind sphere 2 the existing birefringent strands were observed to detach from the surface of the sphere and flow downstream, gradually converging. Also additional birefringent strands were generated around the trailing stagnation point of sphere 2, though these were of reduced intensity to those formed behind sphere 1 and appeared to occupy a smaller volume. A schematic of the observed interaction between the spheres is provided by Fig. 13.

Discussion

It should be remembered when considering the results presented here that the present experiment is subtly

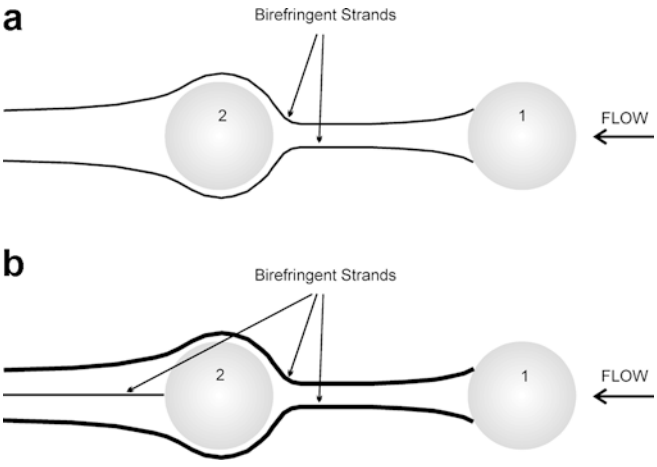

Fig. 13a,b Schematic showing how the birefringent strands develop in the double-sphere cell: **a** at "moderate" flow rates the birefringent strands from the first sphere screen the flow-field in the wake such that $\dot{\epsilon} < \dot{\epsilon}_c$ behind sphere 1 and $\dot{\epsilon} < \dot{\epsilon}_c$ behind sphere 2; **b** at higher flow rates the strain rate can exceed the critical value behind both spheres but is still reduced behind sphere 2 due to increased flow screening

different from the falling ball experiment in various respects.

Since the flow rate in the present experiment is forced to be steady state (for both spheres) the difference in force felt by the spheres results in a fixed separation between them. Also, in the present experiment there is no independent control of flow velocity or initial temporal separation between the spheres: increasing the flow rate has the unavoidable simultaneous effect of reducing the time interval for flow between the spheres. Also, of course, the difference in stress in the two cantilevers results in a slight reduction of the 5-mm gap between the spheres, which further compounds this effect.

There are various reasons why falling ball experiments could not be expected to produce results such as observed here, particularly as regards the magnitude of Δv_{eff}. It is hard to achieve high *De* flows in falling ball experiments because the increase in extensional viscosity has the effect of limiting the strain rate of the experiment (the strain rate is also limited by the force of gravity and the density and buoyancy of available spheres). Even if equivalent strain rates could be achieved, to drop balls with controlled 5-mm (or 1/30 s) gaps between them would be extremely difficult.

In a falling ball experiment the different viscous forces felt by two spheres falling along the same path would result in different sphere velocities. If the difference in velocity could be as great as Δv_{eff} suggests, this would result in a rapid change in the distance between the spheres. If sphere 2 fell faster than sphere 1, the 5-mm gap between the spheres would quickly reduce and the spheres would eventually converge. This was observed in the experiments of Riddle et al. (1977).

Whilst 5 mm or 1/30 s is very small compared to previous studies (Bisgaard 1983; Cho et al. 1984; Jones et al. 1994), it should be remembered that here we are using highly dilute solutions of very low τ.

Although there are subtle complications in the analogy between the falling ball experiment and the present study, since the flow geometries of the two experiments are virtually identical and the non-Newtonian effects that are observed in both experiments are clearly equivalent, conclusions drawn from the present study can certainly be applied to the falling balls.

It has been shown that the specific viscosity of dilute a-PS/DOP solutions can increase significantly when flowing around a sphere beyond an onset Deborah number. Considering the lower concentrations of the solutions in the present study, the increases in specific viscosity are consistent with the increases in drag coefficient reported by Solomon and Muller (1996).

As mentioned above, the force and specific viscosity curves obtained from the a-PS/DOP solutions are similar in form to the results of Carrington et al. (1997a, 1997b), for a 0.02% solution of $M_w = 8\times10^6$ a-PS in dekalin in the opposed jets. The increase in viscosity between the jets observed by Carrington et al. was confirmed as being due to the coil↔stretch transition postulated by de Gennes (1974) and Hinch (1977) as it coincided with the increase in birefringence between the jets.

The images of birefringence presented here (see Fig. 6) also confirm that a-PS molecules in solution can accumulate significant strain near the stagnation point of a sphere at Deborah numbers where there is an increase in the specific viscosity of the solution. Semi-quantitative estimates of the birefringence show that at sufficient dilution and strain rate, close to full molecular strain can occur. There is a reasonable correlation between the onset *De* for the viscosity increase and the onset *De* for the appearance of a birefringent signal. Therefore it is reasonable to make the assumption that the increase in specific viscosity felt by the spheres in a-PS solutions is due to the accumulation of molecular strain, i.e. an increase in the extensional viscosity of the solution.

Logically, the stagnation point appears to be the most crucial region where polymer molecules accumulate strain, since in the locality of the stagnation point molecules will experience the longest residence time in the extensional flow field and are subjected to a high strain rate. Evidently polymer molecules remain highly stretched as they flow away from the sphere along the stagnation point streamline.

Hysteresis in the coil↔stretch transition may play a crucial role in maintaining the molecules in the stretched conformation. As predicted by de Gennes (1974), the relaxation time of a highly coiled polymer molecule may increase when the molecule is stretched due to increased

viscous contacts between the polymer chain and the solvent molecules. Therefore a molecule that becomes stretched in the stagnation point behind a sphere may have to flow for some distance away from the stagnation point before the strain rate becomes sufficiently low for the molecule to relax again.

The results of the flow visualization study show that the flow along the symmetry axis in the wake of the sphere can be considerably perturbed by the presence of the polymer additives in the solution. It must be assumed that the strands of highly stretched birefringent polymers in the wake of the sphere are the cause of these large alterations to the flow dynamics. A single localized birefringent line emanating from the trailing stagnation point causes a reduction in the strain rate at the stagnation point due to the increase in extensional viscosity. The presence of this strand will affect the flow dynamics such that the point of greatest strain rate is moved radially away from the symmetry axis of the flow (i.e. the stagnation ''point'' may effectively become a ring centred on the stagnation point), so that the birefringent strand gets broader with increasing flow rate. As *De* increases and the birefringence spreads in a radial direction from the stagnation point streamline, the flow along the stagnation point streamline becomes increasingly screened from the bulk flow field. Eventually the flow velocity in the centre of the birefringent strand may become reduced such that the macromolecules there cannot stretch, resulting in the complex birefringent structures that are observed. This is essentially the same as was predicted by Harlen et al. (1992), who used a FENE dumbbell model with non-linear hydrodynamic friction to show how birefringent pipe structures could form in the flow of dilute polymer solutions near stagnation points.

Our measurements of the flow field around the single sphere are qualitative; however they show a similar form to the detailed measurements of Fabris et al. (1999) for spheres falling in a 0.16% solution of $M_w = 20\times10^6$ a-PS in a viscous solvent. The important message of our flow visualisation study is that the flow field in an a-PS solution can be significantly perturbed from a Newtonian type flow field by the stretching of polymer molecules behind the sphere, even at very high dilution.

It seems reasonable to conclude that the excess stress felt by the sphere in an a-PS solution (compared with the solvent) is supported by the strain in the polymer molecules in the wake of the sphere. There are two reasons why stretched polymers in the wake may contribute to the force experienced by the sphere. First, the stretched polymeric material in the wake can be thought of as an elastic strand connected to the stagnation point and trailing behind the sphere. Viscous forces between the birefringent strand and the flowing solution will therefore contribute to the drag force on the sphere. Second, entropic elastic forces are also likely to be significant since the polymers in the birefringent strand are constantly striving to return to a randomly coiled conformation, which will pull the sphere towards the direction of flow.

The accumulation of strain by the polymer molecules near the stagnation point in the single sphere flow cell (visible as birefringence) is therefore responsible for the increase in the apparent viscosity of the solution, which has the additional effect of causing modifications to the Newtonian flow field in the wake of the sphere. The resulting interaction between the flow modification and the polymer stretch may help to create the long wake behind the sphere by maintaining a velocity gradient along the stagnation streamline for several sphere radii downstream.

This interaction is also likely to be the cause of flow instabilities in the wake of the sphere at high *De*. The stretching polymers modify the flow, which affects the polymer stretch. This in turn modifies the flow further, resulting in the rapid fluctuation in the birefringent structure, i.e. essentially visco-elastic instabilities. It should be noted that Harris and Rallison (1994) have suggested a similar explanation for the occurrence of flow instabilities near an isolated stagnation point in dilute dumbbell solutions incorporating non-linear hydrodynamic friction. Flow instabilities of this type have also been observed in flow of a 0.25% solution of $M_w = 1.92\times10^6$ PS in a viscous solvent past a rear stagnation point in a study by Li et al. (2000).

In the double sphere flow cell, the specific viscosity vs *De* curves for the a-PS solutions indicate that polymer molecules undergo a coil↔stretch transition in the wakes of both spheres. However the viscosity increase for sphere 2 generally occurs at a higher strain rate than for sphere 1 and does not reach such a great plateau value.

Observations of birefringence in the wake of sphere 2 indicate that the onset of molecular stretching is delayed to higher strain rate than in the single sphere flow cell. Also, for a given strain rate, the intensity of the birefringence is lower in the wake of sphere 2 than it is in the wake of sphere 1, which indicates that the polymers there do not accumulate such a high degree of strain.

The specific viscosity curves and observations of birefringence in the double sphere cell are therefore consistent with each other and support the hypothesis that the excess force experienced by the spheres in polymer solutions, compared to the solvent, is due to the accumulation of strain in the polymer molecules that pass near the trailing stagnation points.

The birefringent lines coming from sphere 1 are evidently quite stable, as they are long lived on the timescale of the molecular relaxation time and are not destroyed by the flow field that surrounds sphere 2. The birefringent lines are probably best imagined as highly viscous and elastic oriented fibres or strands ''attached'' by one end

to the stagnation point of the sphere. The extensional viscosity of the strands can be hugely increased by the presence of highly extended molecules (Carrington and Odell 1996). However, the strands can also be thought of as highly elastic, as there is a strong entropic restoring force arising in the stretched macromolecules. This description of the birefringent strands provides explanations for both the increased drag force experienced by the spheres above De_o and the flow modification in the wake seen in the single sphere flow cell.

Since the local fluid velocity in the wake of sphere 1 is known to be reduced from the Newtonian value by the presence of the polymer and the viscous birefringent strands have been observed to follow the streamlines around sphere 2, the velocity effect can thus be explained. It appears that sphere 2 effectively becomes confined inside a slow moving, close-fitting, birefringent tube, formed from the strands originating from sphere 1. Inside the tube sphere 2 encounters fluid in which the polymer molecules are un-stretched. Also the flow velocity of fluid inside the birefringent tube is reduced from the bulk flow rate due to screening of the flow field by the extension-resisting strands.

The reduction in flow velocity in the wake of sphere 1 may partially account for the velocity effect; however, the screening of the flow field around sphere 2 also means that sphere 2 effectively experiences a lower Deborah number than sphere 1. Hence sphere 2 experiences the increase in extensional viscosity at a higher volume flow rate than sphere 1. For a given volume flow rate less of the polymer molecular weight distribution will stretch behind sphere 2 than sphere 1, so the birefringence will be lower resulting in a smaller increase in the apparent extensional viscosity.

Conclusions

We have shown that monodisperse polymer molecules in dilute solution stretch in flow around a sphere beyond an onset strain rate or Deborah number. The most important region in the flow field for the accumulation of molecular strain is the trailing stagnation point of the sphere, where the strain rate is high and the residence time is long, so that accumulated strains can be close to full extension of the macromolecules. The effect is to produce a birefringent strand in which the highly stretched molecules give rise to an appreciable increase in the extensional viscosity of the polymer solution, coupled with a high entropic elastic restoring force. The strands extend over long times and length scales, which we attribute to hysteresis in the coil↔stretch, stretching and relaxation processes.

At concentrations well below the conventional critical overlap concentration, c^*, the increase in extensional viscosity and elasticity in the wake of the sphere, due to the presence of stretched polymer molecules, dramatically affects the local flow field in the wake. The interactions between the modified flow-field and the polymer stretch help to maintain the extended wake far downstream of the sphere and, at high *De*, give rise to complex birefringent structures and flow instabilities.

The apparent onset Deborah number for polymer stretching at the stagnation point of a downstream sphere (sphere 2) is increased compared to the first sphere to encounter the flow (sphere1). Beyond the onset Deborah number the extensional viscosity of the polymer solutions increases to a higher apparent value for flow around sphere 1 than for sphere 2. The differences in the estimates of extensional viscosity between the spheres are consistent with the observations of birefringence of greater intensity and radial dimension behind sphere 1 than behind sphere 2. The differences in extensional viscosity and birefringence can be explained by screening of the flow field around sphere 2 by the highly viscous and elastic birefringent strands originating from the stagnation point of sphere 1. We suggest this as a mechanism for the ''velocity effect'' anomalies in some falling ball systems.

These mechanisms are likely to be of major relevance to the viscosification mechanism in porous media flow. The double sphere results show a marked reduction in the effectiveness of the down-stream stagnation points in aligned systems due to screening effects. This might have profound implications for modelling of porous media by close-packed arrangements of spheres, because local crystallographic arrangements are likely to result in alignment and therefore reduce the effectiveness of stagnation points (Haward and Odell 2003).

Acknowledgements We gratefully acknowledge the support of EPSRC and the EU Alfa programme. We are indebted to Dr S.P. Carrington for helpful discussions.

References

Arigo MT, Rajagopalan D, Shapley N, McKinley GH (1995) The sedimentation of a sphere through an elastic fluid. Part 1. Steady motion. J Non-Newtonian Fluid Mech 60:225–257

Berry GC (1967) Thermodynamic and conformational properties of polystyrene. II. Intrinsic viscosity studies on dilute solutions of linear polystyrene. J Chem Phys 46:1338–1352

Bisgaard C (1983) Velocity fields around spheres and bubbles investigated by laser-Doppler velocimetry. J Non-Newtonian Fluid Mech 12:283–302

Carrington SP, Odell JA (1996) How do polymers stretch in stagnation point extensional flow-fields?. J Non-Newtonian Fluid Mech 67:269–283
Carrington SP, Odell JA (2003) Extensional flow oscillatory rheometry. J Rheol (submitted)
Carrington SP, Tatham JP, Odell JA, Saez AE (1997a) Macromolecular dynamics in extensional flows. 1. Birefringence and viscometry. Polymer 38:4151–4164
Carrington SP, Tatham JP, Odell JA, Saez AE (1997b) Macromolecular dynamics in extensional flows. 2. The evolution of molecular strain. Polymer 38:4595–4607
Cathey CA, Fuller GG (1990) The optical and mechanical response of flexible polymer solutions to extensional flow. J Non-Newtonian Fluid Mech 34:63–88
Chhabra RP, Uhlherr PHT (1979) Estimation of zero-shear viscosity of polymer solutions from falling sphere data. Rheol Acta 18:593–599
Chilcott MD, Rallison JM (1988) Creeping flow of dilute polymer solutions past cylinders and spheres. J Non-Newtonian Fluid Mech 29:381
Cho YI, Hartnett JP, Lee WY (1984) Non-Newtonian viscosity measurements in the intermediate shear rate range with the falling-ball viscometer. J Non-Newtonian Fluid Mech 15:61–74
de Gennes PG (1974) Coil-stretch transition of dilute flexible polymers under ultra-high velocity gradients. J Chem Phys 60:5030–5042
Degand E, Walters K (1995) On the motion of a sphere falling through an elastic liquid contained in a tightly-fitting cylindrical container. J Non-Newtonian Fluid Mech 57:103–115
Durrans TH (1971) Solvents, 8th edn. Chapman and Hall, London
Fabris D, Muller SJ, Liepmann D (1999) Wake measurements for flow around a sphere in a viscoelastic fluid. Phys Fluids 11:3599–3612
Gottlieb M (1979) Zero-shear-rate viscosity measurements for polymer solutions by falling ball viscometry. J Non-Newtonian Fluid Mech 6:97–109
Graessley WW (1980) Polymer chain dimensions and the dependence of viscoelastic properties on concentration, molecular weight and solvent power. Polymer 21:258–262
Harlen OG (1990) High-Deborah-number flow of a dilute polymer solution past a sphere falling along the axis of a cylindrical tube. J Non-Newtonian Fluid Mech 37:157
Harlen OG, Rallison JM, Chilcott MD (1990) High-Deborah-number flows of dilute polymer solutions. J Non-Newtonian Fluid Mech 34:319–349
Harlen OG, Hinch EJ, Rallison JM (1992) Birefringent pipes: the steady flow of a dilute polymer solution near a stagnation point. J Non-Newtonian Fluid Mech 44:229–265
Harris OJ, Rallison JM (1994) Instabilities of a stagnation point flow of a dilute polymer solution. J Non-Newtonian Fluid Mech 55:59–90
Haward SJ, Odell JA (2003) Viscosity enhancement in non-Newtonian flow of dilute polymer solutions through crystallographic porous media. Rheol Acta 42:516–526
Hinch EJ (1977) Mechanical models of dilute polymer solutions in strong flows. Phys Fluids 20:S22–S30
Jones WM, Price AH, Walters K (1994) The motion of a sphere falling under gravity in a constant-viscosity elastic liquid. J Non-Newtonian Fluid Mech 53:175–196
Leal LG, Denn MM, Keunings R (1988) Lake Arrowhead workshop special issue papers. Introduction. J Non-Newtonian Fluid Mech 29:1–8
Li J-M, Burghardt WR, Yang B, Khomami B (2000) Birefringence and computational studies of a polystyrene Boger fluid in axisymmetric stagnation flow. J Non-Newtonian Fluid Mech 91:189–220
Peterlin A (1961) Streaming birefringence of soft linear macromolecules with finite chain length. Polymer 2:257–264
Riddle MJ, Narvaez C, Bird RB (1977) Interactions between two spheres falling along their line of centres in a viscoelastic fluid. J Non-Newtonian Fluid Mech 2:23–35
Solomon MJ, Muller SJ (1996) Flow past a sphere in polystyrene-based Boger fluids: the effect on the drag coefficient of finite extensibility, solvent quality and polymer molecular weight. J Non-Newtonian Fluid Mech 62:81–94
Treloar LKG (1975) The physics of rubber elasticity, 3rd edn. Clarendon Press, Oxford